Applied Nanoscience
https://doi.org/10.1007/s13204-020-01255-8

ORIGINAL ARTICLE

PEGylation of graphene/iron oxide nanocomposite: assessment of release of doxorubicin, magnetically targeted drug delivery and photothermal therapy

Marzieh Ramezani Farani[1] · Parissa Khadiv-Parsi[1] · Gholam Hossein Riazi[2] · Mehdi Shafiee Ardestani[3] · Hamidreza Saligheh Rad[4,5]

Received: 11 September 2019 / Accepted: 4 January 2020

Abstract

Scientists have recommended to investigate graphene and graphene base compounds for their potential uses in a variety of fields, such as biomedicine and drug release. A PEGylated and functionalized magnetic graphene oxide (MG–NH_2–PEG) complex was used herein as a nanocarrier of Doxorubicin, a cancer chemotherapy drug. First, graphene oxide was synthesized by modified Hummer's method and then functionalized with amine groups (G–NH_2). Afterwards, solvothermal of Fe_3O_4 magnetic nanoparticles on G–NH_2 to prepare magnetic graphene oxide (MGO) modified by MG–NH_2 via covalent bindings for the synthesis of MG–NH_2–PEG. Doxorubicin (DOX) was loaded onto MG–NH_2–PEG at pH 7 by the use of π–π interactions, yielding a highly significant value of DOX's loading efficiency along with its loading content. In vitro cytotoxicity tests on MCF-7 cells line were carried out for MG–NH_2–PEG: DOX according to the drug loading and release characteristics. The results of standard MTT assay for the toxicity determination of both synthetic nanocomposites and the drug revealed over 85% of surviving cells after 48 h, with a cellular uptake of > 80%, suggesting a satisfactory outcome on the non-toxicity of the nanocomposite. It can, therefore, be concluded that MG–NH_2–PEG showed to be an effective drug carrier in cancer chemotherapy drug delivery through loading the above drugs of low medicinal properties with individual dependency on pH levels. Furthermore, MG–NH_2–PEG represent strong optical absorbance from the visible to the near-infrared (NIR) region, and can be utilized for localized photothermal ablation of cancer cells guided by the magnetic field.

Keywords Graphene oxide · Superparamagnetic iron oxide nanoparticles (SPIONs) · Pegylation · Magnetically targeted drug delivery · Photothermal therapy · Doxorubicin

✉ Parissa Khadiv-Parsi
kparsi@ut.ac.ir

✉ Mehdi Shafiee Ardestani
shafieeardestani@tums.ac.ir

1 School of Chemical Engineering, University College of Engineering, University of Tehran, Tehran 4563-11155, Iran

2 Institute of Biophysics and Biochemistry, University of Tehran, Tehran 1417614411, Iran

3 Department of Radio-Pharmacy, Faculty of Pharmacy, Tehran University of Medical Sciences, Tehran 1417614411, Iran

4 Quantitative Medical Imaging Systems Group, Research Center for Molecular and Cellular Imaging, Tehran University of Medical Sciences, Tehran 1417613151, Iran

5 Medical Physics and Biomedical Engineering Department, Tehran University of Medical Sciences, Tehran 1417613151, Iran

Introduction

A major research field in nanomedicine has been the application of therapeutic nanocarriers in recent years (Skwarecki et al. 2016). Various methods have been employed to prepare nanocarriers with the aim of a safe and effective cell-targeting function, of which the findings indicate a high potential for anticancer drug delivery (Feng and Liu 2011). The ability of nanocarriers in controlled drug release during a continuous period is another fascinating application among lots of potential treatments for cancer, diabetes, chronic pain, and so on (Garg et al. 2015; Guo 2016). Our apprehension of physicochemical properties of drug molecules and the progressive understanding of cellular uptake mechanisms arise from important developments in drug manufacturing for various diseases, which have resulted in extensive and operative therapies (Depan et al. 2011; Liu et al. 2018).

Published online: 30 January 2020

Effective drug doses can be conveyed to target tissue cells by a capable targeted drug delivery system. The biocompatibility of carriers determines the success of this approach enabling large amounts of drug molecule loading with no early cargo unloading prior to reaching the target (Huang 2012). For drug delivery systems, biocompatibility is the most important feature (Guo 2016; Depan et al. 2011; Liu et al. 2018; Huang 2012; Liao et al. 2011). Biomedical applications use various types of organic and inorganic nanomaterials as drug carriers typically including liposomes, dendrimers, carbon nanotubes, and gold nanoparticles (Zhao et al. 2016; Mohammad-Taheri et al. 2012).

Graphene is a biodegradable carbon nanomaterial containing sp^2 hybridized carbon atoms in a 2D structure, which has been in the focus of scientists worldwide as a drug delivery substance (Dissanayake et al. 2015; Kiew 2017; Lu et al. 2012; Ma 2012) owing to its outstanding mechanical (Sablok et al. 2013), electrical (Mehnati-najafabadi et al. 2018) thermal (Singh et al. 2012), and optical properties (Yuan et al. 2014) as well as a high surface area (Ge 2014). The dispersion and adaption of graphene can be enhanced using different matrices of graphene oxide (Ozcan et al. 2009; Cole et al. 2011; Li et al. 2017). Graphene nanosheets possess high drug loading rates shoeing a high surface property, π–π accumulation and hydrophobic interactions, hence, being a superb choice for anticancer drugs/gene delivery, biological sensors and bio-imaging, antibacterial applications, cell culture, and tissue engineering, providing a suitable modification (Guo 2016; Farani and Press 2019; Qiao et al. 2018; Markovic 2011).

A number of graphene composite nanomaterials made of graphene or graphene oxide in combination with various types of nanoparticles have greatly been used in a vast variety of energy applications, catalysts and other fields of research, in addition to graphene oxide or pure graphene (Markovic 2011). As detected by Wu et al. the release kinetics of Doxorubicin values and the synchronization with photothermal properties was enhanced by synthesized golden nanorods/graphene oxide (Hong et al. 2011). Synthesized polyethylene glycol coated with MGO nanocomposite was found by Sasikala et al. to be appropriate for cancer therapy owing to plenty of therapeutic functions besides MRI imaging capabilities (Marković 2017).

A recent study has demonstrated that graphene oxide/magnetite/gelatin coated nanocomposite (GO–IONP–PEG) used as an enhancer of the T_2 contrast phase of MRI images can be applied for Doxorubicin delivery (Ozcan et al. 2009). The synthesis of GO/Fe_3O_4/Au/PEG nanocomposites aimed at a high enrichment of glycopeptides (Angelopoulou et al. 2015).

The pH-dependent drug release function categorized for chemotherapeutic drug release in the GO group is advantageous because of improving drug delivery under a low pH level (pH 5–5.5), ultimately providing an effective drug release for intercellular conveys (Su et al. 2019; Wilding et al. 2018). The synthesis of polyethene glycol coated GO nanoparticles with a real capability for magnetic nanoparticles indicates the ability of pH-controlled releasing method and the magnetic target to surmount the limitation of GO-based drug delivery systems (Ma 2012; Sun et al. 2018). The magnetic drug-loaded nanoparticles can be inserted into malignant tumors area by the magnetic field and the completion of endocytosis process by tumor cells is followed by the relief of related side effects (Dinesh et al. 2017; Baniasadi et al. 2015).

As a commonly administered drug for various cancer chemotherapy, Doxorubicin (DOX) successfully targets and eliminates cancer cells through inhibition of topoisomerase II, DNA chelation, and hydroxyl radical effect (Kumawat et al. 2017). This therapy course, however, involves such various fallouts as hair fall, qualmishness, disgorging, myocardial injuries, and tissue inflammation.

MG–NH_2–PEG was used in here to deliver DOX according to chemical co-precipitation method (Su et al. 2019; Wilding et al. 2018). MG–NH_2–PEG: DOX underwent in vitro cytotoxicity tests against on MCF-7 cells line based on the characteristics of drug loading and release.

Experimental

Materials

Graphite powder, ethanol, iron (III) chloride hexahydrate 98% ($FeCl_3{\cdot}6H_2O$), *N*-(3dimethylaminopropyl-*N*-ethylcarbodiimide) hydrochloride (EDC), *N*-hydroxy succinimide (NHS), sodium acrylate (CH_2=CHCOONa), sodium acetate (NaOAc), ethylene glycol (EG), triethylamine (TEA), diethylene glycol (DEG), thionyl chloride ≥ 99% ($SOCl_2$), dimethyl formamide (DMF), methylene chloride (CH_2Cl_2), sodium azide (NaN_3), hydrochloric acid (HCl), poly(ethylene glycol) bis(carboxymethyl) ether (average Mn 600), sodium nitrate ($NaNO_3$), hydrogen peroxide (H_2O_2), sulfuric acid and potassium permanganate were obtained from Sigma Aldrich.

Doxorubicin was acquired from Pakhsh Razi Co., Ltd, Tehran, IRAN. The Iranian Pasteur Institute provided murine breast cancer MCF-7 cell line. All cell culture reagents and thiazolylblue tetrazolium bromide (MTT) were purchased from Sigma–Aldrich.

Methods

Preparation of graphene oxide (GO)

The graphite-based graphene oxide was prepared by a modified Hummer's method (Yuan et al. 2014; Kumawat et al. 2017). First, graphite (0.5 g) and $NaNO_3$ (0.5 g) were mixed

and stirred at 300 rpm for 30 min at a temperature < 20 °C in the ice bath. Then 98% sulfuric acid (23 ml) was added to the mixture with similar ambient condition and stirred for a further 4 h. Afterwards, $KMnO_4$ (3 g) was added gently for 2 h. Next, the ice bath was taken out and thermal condition was raised from 20 °C to 98 °C followed by addition of H_2O_2 to the resultant biphasic solution, with water in the upper phase and the underneath golden powder. Hydrochloric acid 5% (w/w) was added after removal of the upper phase and then stirred for 1 h, the whole process was repeated thrice. Deionized water was added in lieu of hydrochloric acid in the third trial with duplicated activities. The procedure was repeated to the point that no other two phase solutions were present and when the sediment stability was observed in water. The final solution was poured into centrifugal falcons and centrifuged at 40000*g* at separate times (1.0 h) and at ambient temperature along with reading the pH. Following seven rounds, the pH rose from 1.2 to 4.8, as very expedient outcome. The resultant concentration of the precipitate was 0.45 g suggesting the stability of graphene oxide solution, which was dried at 60 °C.

Synthesis of G–NH2

To examine amine functionalization (G–NH_2), GO (1.0 g) was mixed with $SOCl_2$ (60 ml) under ultrasonic conditions for 2 h. Then DMF solvent (3 ml) was poured into the suspension with raising the temperature to 70 °C, which lasted 24 h under gas flux N_2. The obtained arrangement maintained in the last condition.

After ceasing the gas flux and declining the temperature as low as 0 °C, DMF (120 ml), TEA (10.1 g), and NH_3H_2O (5.0 g) were added to the above mixture for 1 h. The final solution was purified by a pencil of PTFE membrane filter (pore size 0.22 µ) and rinsed with ammonia several times (Costantini et al. 2013).

Synthesis of MG–NH2

Two isolated solutions, one containing G–NH_2 (20 mg), $FeCl_3{\bullet}6H_2O$ (270 mg), sodium acrylate (750 mg) and sodium acetate (750 mg), and the other one holding ethylene glycol (0.5 ml) and diethyl glycol (9.5 ml) were first prepared in this phase of the experiment. This was followed by combining both solutions to obtain a homogeneous solution that was transferred to a stainless steel autoclave for storage in a furnace at 200 °C for 12 h. The resultant solution (MG–NH_2) was rinsed repeatedly with water and ethanol solution and finally dried under vacuum condition for 15 h (Ozcan et al. 2009).

Attempts were made to measure Fe concentration in MG–NH_2, for which a ratio of 1:2.33 was estimated concordant to the plasma content ICP test.

Synthesis of MG–NH_2–PEG

At first, enough ammonium solution with 25% concentration was added to increase the pH of solution to 8. Subsequently, 100 µl of poly (ethylene glycol) bis (carboxymethyl) ether (600 Da) was added to MG–NH_2 solution (25 ml) and sonicated for 15 min. The solution then received 10 mg of N-Hydroxy succinimide (NHS), and 15 min later, 30 mg of *N*-(3-dimethylaminopropyl-*N*'-ethylcarbodiimide), hydrochloride (EDC). Finally, the reaction vessel was wrapped by aluminum foil and kept agitated nightlong at room temperature. The MG–NH_2–PEG as the final product was purified with a Dialysis bag (5KDa) for 24 h to eliminate unreacted PEG and other reagents (Hu et al. 2014).

Synthesis of MG–NH_2–PEG

Initially, a 25% concentration of ammonium solution was added to elevate the pH of solution to 8. Then, 100 µl of Poly (ethylene glycol) bis (carboxymethyl) ether (600 Da) was poured into MG–NH_2 solution (25 ml) and sonicated for 15 min. Then 10 mg of *N*-hydroxy succinimide (NHS) and 15 min later, 30 mg of *N*-(3-dimethylaminopropyl-*N*'-ethylcarbodiimide) hydrochloride (EDC) were added to the solution. Finally, the reaction vessel was wrapped with aluminum foil and agitated all-night at room temperature. The MG–NH_2–PEG as the final product was purified with a dialysis bag (5KDa) for 24 h to eliminate unreacted PEG and other reagents (Hu et al. 2014).

Doxorubicin (DOX) loading and DOX release

Various amounts of DOX drugs (0.2–1.6 mg) and MG–NH_2–PEG (0.2 mg/ml) was added to PBS (20 ml) with 20 mmol/l in order to load the MG–NH_2–PEG nanocarrier with the DOX drug. By addition of ammonia, the pH of these solutions was raised up to 8, stirred at 300 rpm for 24 h, then the unreacted DOX was removed from the solutions through a centrifuge at 14,800 rpm for 10 min. Using deionized water, the solid precipitates from the centrifuge falcons (MG–NH_2–PEG: DOX) were rinsed three times. In the end, homogeneous and uniform solutions were prepared by dispersion of the precipitates in distilled water followed by storage at 4 °C (Ozcan et al. 2009; Ordikhani et al. 2015).

The amount of loaded DOX drug was calculated using a UV765, UV/VIS device (Varian Co) at 490 nm (Mendonça 2016).

Physicochemical properties of nanocarriers

The zeta potential was determined via dynamic light scattering (DLS) with a 90Plus Pals (Brookhaven, US) through diluting the samples to 0.1–0.3 mg/ml in deionized water

(0.5 ml). Transmission electron microscope (TEM) observations were performed using a TEM/HRTEM (JEOL, JEM-2100, Japan) at 100 kV (Xie 2017).

DOX release from MG–NH_2–PEG

The MG–NH_2–PEG: DOX solution (1 mg) was incubated in PBS (1 ml, pH 5 and 7.4) at different times to assess the drug release rate. The amount of DOX released from MG–NH_2–PEG–Dox was collected through centrifugation at 14,800 rpm for 10 min. and measured using UV–VIS absorption spectrometry—Carry 100 Bio (Varian). For an unlimited determination of DOX and MG–NH_2–PEG: DOX, fluorescence spectrum was carried out by Carry Eclips (Varian) (Fig. 1).

To determine infiniteness, DOX and MG–NH_2–PEG: DOX, fluorescence spectra were implemented by Carry Eclips (Varian). To do this, quantum dot samples (0.1–0.3 ml) were diluted in distilled water (≈ 0.5 ml) and tested against the control sample (Akhavan and Ghaderi 2010).

To confirm the bioavailability of a drug-free sample (MG–NH_2–PEG), cytotoxic control tests were accomplished with MCF-7 cells via the same procedure mentioned above.

2.3. Cellular experiments

2.3.1. Cell line

The murine breast cancer MCF-7 cell line was obtained as cultured in RPMI 1640 complemented with 10% fetal bovine serum (FBS) and 1% penicillin/streptomycin (Taylor 2015).

2.3.2. In vitro cytotoxicity of MG–NH_2–PEG: DOX

The MCF-7 cells were treated with different concentrations of free DOX, MG–NH_2–PEG, and MG–NH_2–PEG: DOX for 48 h. This was followed by addition of MTT dye (dissolved in DMSO < 0.1%) with a final concentration of 100 µg/ml and incubated in CO_2 incubator at 37 °C for 4 h. After removal of the medium, the violet crystal was dissolved in DMSO for 30 min (Akbarzadeh et al. 2012). The absorbance was determined by a spectrophotometer at 540 nm and a reference wavelength of 630 nm (BioTek, Winooski, VT, USA).

2.3.3. In vitro experimentation of photothermal therapy

Cell killing for photothermal cancer was accomplished through 2 h incubation of MCF-7 cells with 50 mg/l MG–NH_2–PEG at 37 °C. Next, the cells were irradiated with 1 W/cm^2 power density for about 5 min through the application of an 808 nm optical fiber-coupled diode NIR laser (max. power = 10 W). Afterwards the photothermal ablation, and in order to assess the cell killing efficiency, the authors executed a standard cell viability assessment with the aid of MTT (Depan et al. 2011).

2.3.4. Magnetic targeting of the understudy cells

To perform the in vitro magnetic targeting tests, the researcher placed a magnet centrally underneath the culture dish containing the cells. Then attempt was made to concentrate the previously added MG–NH_2–PEG or MG–NH_2–PEG: DOX in points where the magnet was placed throughout the incubation.

2.3.5. Confocal imaging of the understudy cells

As for the confocal imaging of the understudy cells, a Leica SP5 laser scanning confocal microscope was used. The observed DOX fluorescence was recorded by the utilization of a 488 nm laser that played the role of excitation source. Then we stained the alive and dead cells, respectively, using Calcein and propidium iodide (PI), to perform confocal fluorescence imaging.

Results and discussion

3.1. Characterization of MG–NH_2–PEG

As shown in Fig. 2a, UV–VIS spectroscopy of synthesized graphene oxide revealed a strong absorbance peak at 230-220 nm resulting from the transfer of π–π* aromatic C–C bonds. The ~ 300 nm peak is ascribed to the transfer of n–π* C = O bonds confirming the presence of oxygen-containing functional groups (Depan et al. 2011). This peak is usually removed in the action of ammonium-boron-activated oxide-treated graphene, magnetized operating agent of nitrogen-containing magnetite nanoparticles, and a nitrogen-containing functionalized graphene oxide containing polyethylene glycol coated magnetite nanoparticles (Vila, et al. 2012).

To examine the structure of the synthesized graphene oxide and functionalized GO with amine groups, FT-IR spectroscopy was carried out as depicted in Fig. 2b, c). The O–H tensile oscillation in the hydroxyl group and the tensile oscillation of C–H are reflected in the peaks of 3415 cm^{-1} and 2924 cm^{-1} (Liu et al. 2018). The C=O bond in the carbonyl group or carboxyl group is displayed by the peak nested at ~ 1690 cm^{-1}. Peak 1618 cm^{-1} characterizes the aromatic C=C bond or the absorbed water molecules in the graphene oxide structure. The C–OH oscillation of the carboxyl group, the C–O–C oscillation and the tensile oscillation of C–O in epoxy, respectively, result from the peaks of 1398 cm^{-1}, 1290 cm^{-1} and 1180 cm^{-1}. Accordingly, the presence of oxygen species groups (Costantini et al. 2013)

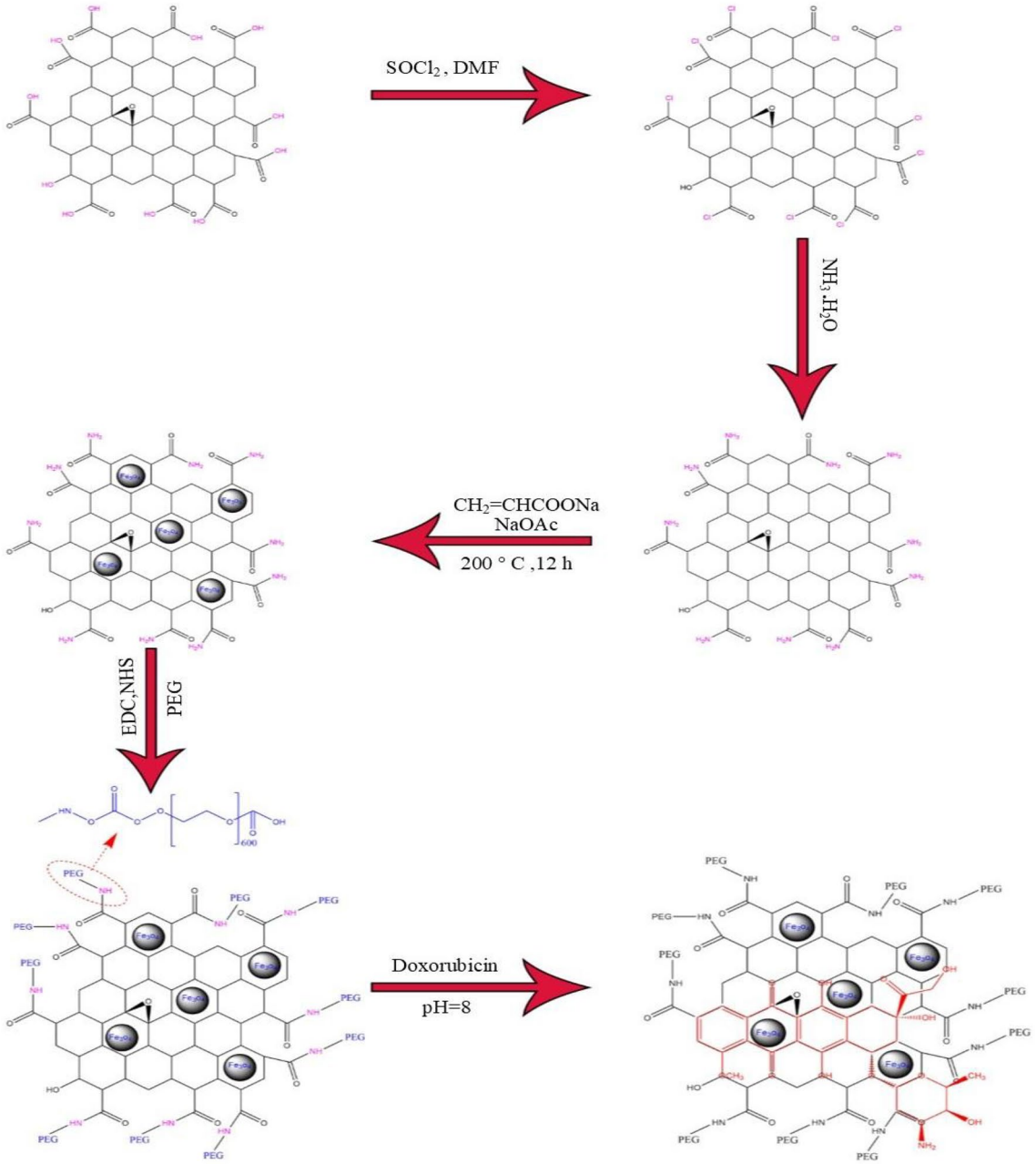

Fig. 1 A schematic of MG–NH_2–PEG synthesis

and successful synthesis of graphene oxide is confirmed by the infrared spectrum of graphene oxide confirms.

The carboxylic groups were replaced by amine groups after functionalization of GO by amine. Figure 2b, c shows a significant peak in the region of 1573 cm^{-1} related to the N–H bond and the peak located within the range of 950–1250 cm^{-1} for the C–N tensile bond. A comparison of two graphene and ammoniated graphene spectra indicated that the peak in the 1735 cm^{-1} region results from the stretching C=O of the carboxylic group (COOH) eliminated in the graphene oxide functionalized with magnetite nanoparticles containing amine groups.

The FT-IR spectrum substantiated an effective polymer (PEGylating)-nanocomposite coupling, which clearly exhibits the strong vibration peaks of the C–H and C–O (Fig. 2b, c).

As shown in Fig. 2b and by comparison of the graphene oxide functionalized with and graphene oxide with amine containing magnetite nanoparticles coated by polyethylene glycol, the vibrating bonds of C–H and CO are reflected in

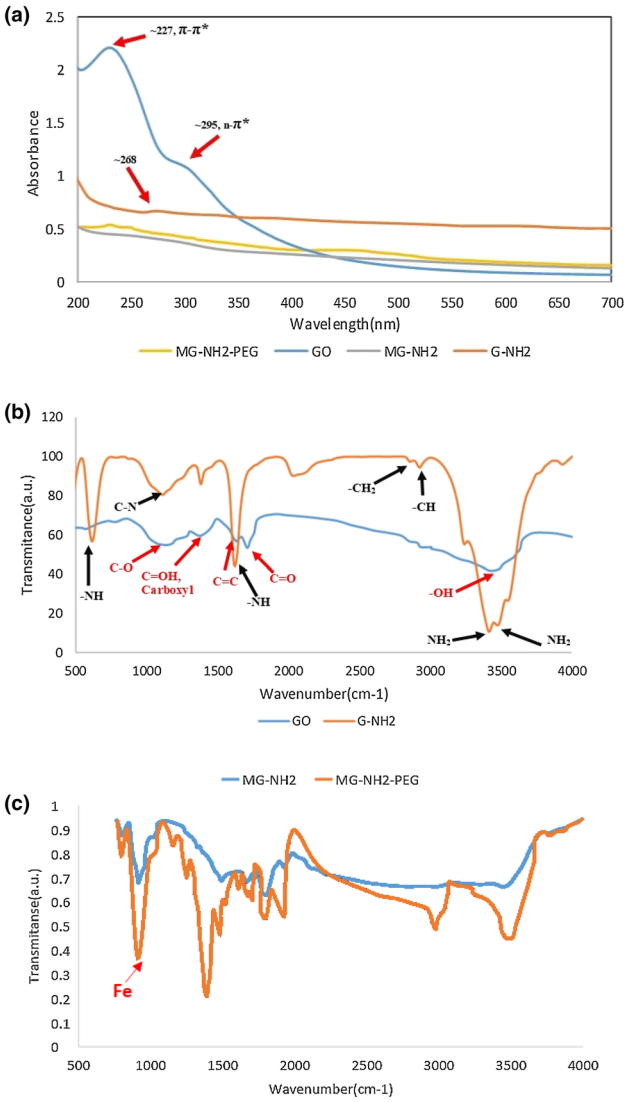

Fig. 2 **a** UV–VIS absorbance spectra of GO, G–NH_2, MG–NH_2 and MG–NH_2–PEG solutions at the same GO concentration (0.01 mg/ml). **b**, **c** FT-IR absorbance spectra of GO, G–NH_2, MG–NH_2 and MG–NH_2–PEG solutions

the peak of 2900 cm^{-1} region and a range of 900–1400 cm^{-1}, demonstrating the association of the polyethylene glycol to the synthetic structure.

Figure 3 illustrates the crystalline structure of graphene oxide examined by X-ray diffraction. The spatial resolution of the plates (002) was detected at about $2\theta = 10.8°$, defined as the distance between the Hammer-synthesized oxide-graphene plates of 2.8 Å based on Bragg's law. A distance of 3.4 Å was observed between the primary graphite plates used for the synthesis of graphene oxide. The presence of oxygen-group groups and water molecules between the graphene oxide plates brings about such a rise in the distance between the graphene oxide plates and the primary graphite.

Tables 1 and 2 represent the calculated particle distance using the Debye Scherrer equation. It clearly indicates that the size achieved for nanoparticles roughly equals the Debye Scherer relation with Bragg's spacing (Akbarzadeh et al. 2012). The type of iron oxide present in the specimens can be identified by comparison of the diffraction pattern acquired from the sample and the reference diffraction patterns (Fig. 3). Various peaks are noticeable in the diffraction pattern to iron oxides. It can be realized that the peak with the highest intensity belongs to the plane via comparison of the reference peaks for Fe_2O_3 and Fe_3O_4 (311). The second and third peaks are located in the diffraction patterns of each material in different positions (with regard to intensity). The second peak is in terms of the magnitude of the page (440) and the third peak of the page (220), whereas it shows the dislocation of hematite. To determine the type of iron oxide linked to Fe_3O_4 particles, the reference diffraction patterns can be used via comparison of the diffusion pattern attained from the synthesized nanoparticles. The specified peaks conform to the JCPDS Reference No.89-3854 Fe_3O_4 Reference Corps, demonstrating a successful synthesis.

The synthesis of MG–NH_2–PEG nanocomposite was achieved with chemical precipitation of iron oxide nanoparticles on soluble amino acid graphene water sheets. As represented in Fig. 3, the presence of cubic Fe_3O_4 nanocrystals in the nanocomposite was established by X-ray diffraction data (XRD). It was dissolved in water and rapidly amassed in

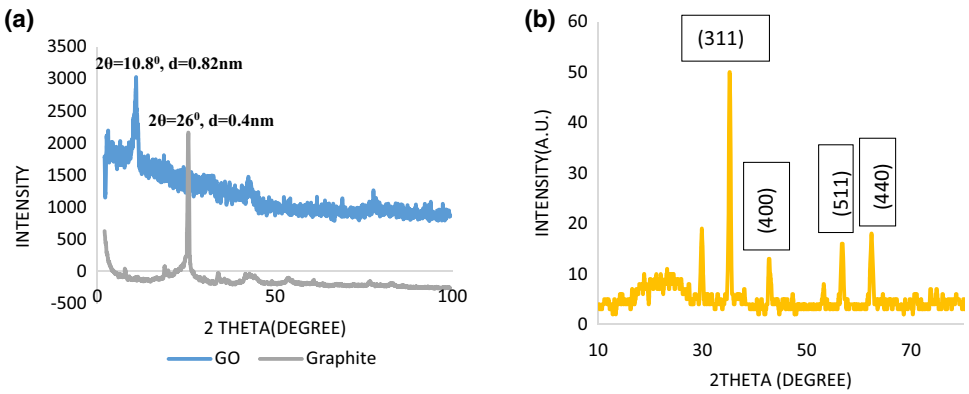

Fig. 3 X-ray diffraction pattern of **a** graphite and graphene oxide sheets synthesized by Hummer. **b** MG–NH_2–PEG

Table 1 The grid radius of the calculated graphene from the Debye Scherrer relationship

Angel (2θ)	11.38	22.9	25.52	29.7	31.9	42.42	52.3
Size (nm)	0.071	0.02	0.141	0.282	0.119	0.245	0.153

Table 2 The distance between the magnitudes of the particles calculated from the Debye Scherrer relations

Angel (2θ)	30.36	35.72	43.39	53.79	57.38	62.98
Size (nm)	0.18	0.176	0.211	0.195	0.148	0.132

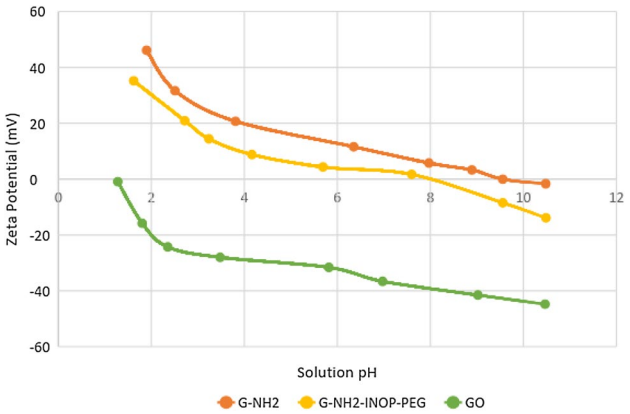

Fig. 4 Zeta potential measurements

the presence of salt, however, it cannot be applied in biological systems. Different physiological solutions (e.g., saline, cellular cells and serum from polyethylene glycol polymer) have benefitted from this method for the stabilization of the nanocomposite.

Figure 4 indicates measurements of zeta potential to find out the levels of graphene surface charges. According to the results, GO sheets have negative charges in the pH values of 3.5 and 9, likely caused by the presence of COOH groups on the surface of graphene. G–NH_2, On the other hand, was positively charged in pH levels of < 10. Furthermore, the observation of properties in a high-pH environment might have resulted from the presence of carboxylic acid groups. In a pH level of 8.2, the zeta-potential value of polymerized nanoparticles approximated zero, which corresponded to the dropped oxygen functional groups (Fig. 4).

3.2. Magnetic properties of MG–NH_2–PEG

As shown in Fig. 5a, the MG–NH_2–PEG morphology was studied through TEM. The graphene oxide screen has an area of 600–800 nm, which is entirely covered with magnetite nanoparticles.

Expectedly, a super-paramagnetic function was seen for the magnetite nanoparticles (Fig. 5b). As reported by earlier studies, the magnetite mass has a magnetization saturation of 92 emus/g (Jiang 2013). According to our findings, graphene oxide was 31.052 emu/g when functionalized with amine groups of magnetite nanoparticles, and it was 4.595 emu/g for graphene oxide functionalized with amine group containing magnetite nanoparticles covered with polyethylene glycol. Thus, the absence of a polyethylene glycol covering in a sample leads to higher magnetized coatings as opposed to a coated sample. The magnetic properties of the nanoparticle may be reduced by non-magnetic material coating (El-boubbou 2018). Magnetic properties are higher in non-coated samples being a robust fact to be used in MRI fields, however, such samples do not dissolve in the aquatic environment, hence, hindering their usage in clinical applications. These data further denote that the magnetization saturation of both samples is in a field of about 10000Oe (1A/m), which is satisfactory MRI uses as well (1.5 T) (Tao et al. 2019).

3.3. Drug loading and release with MG–NH_2–PEG

Using the method described in synthetic nanocomposite, DOX was loaded as an anticancer drug. The nanocomposite MG–NH_2–PEG: DOX completely dissolves in water. As shown by previous investigations, aromatic amphoteric molecules (containing aromatic rings) can pile up on the surface of carbon-2-n nanomaterials (e.g., carbon nanotubes and grapheme) with π–π interaction (Ma 2012). Figure 1 displays loading of DOX with MG–NH_2–PEG as a nanocarrier that was simply scattered in water and turned the solution into a clear red color. Figure 6a depicts the UV–VIS spectra of the sample loaded with DOX and the unloaded sample. The spectrum implies that DOX drug has an absorption peak at 490 nm. Moreover, Fig. 6b exhibits the fluorescence spectrum of two samples.

The amount of DOX loading on the nanocomposite was determined through addition of MG–NH_2–PEG solution to different DOX values (pH 8). When unwanted DOX was removed excessively, an increased DOX loading efficiency was seen from 44% to ~ 220% (DOX to nanocarrier weight ratio) via elevating the amount of DOX added in the form DOX loading (~ 100%), which was chosen by MG–NH_2–PEG: DOX weight ratio of 1 to 2 for the present

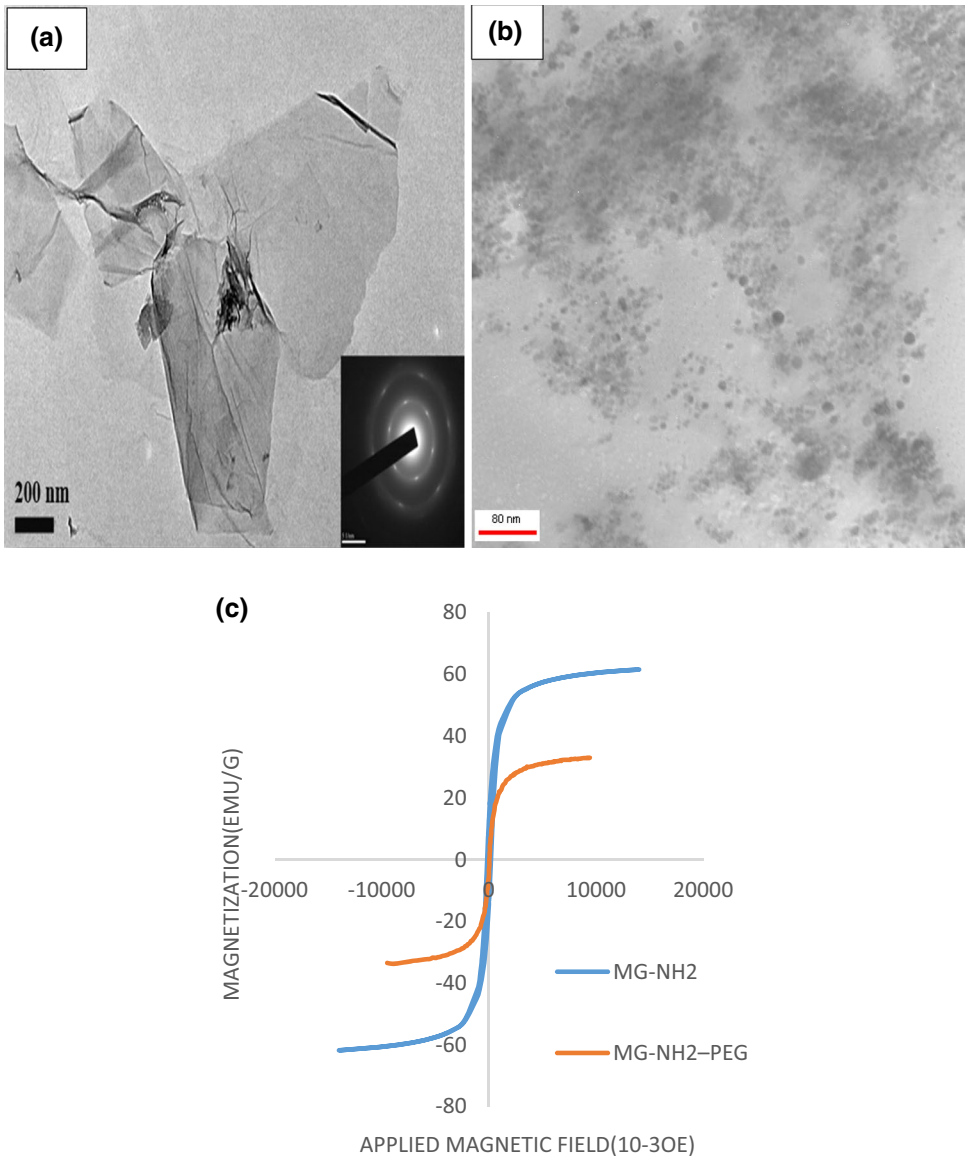

Fig. 5 Microscopic characterization: TEM images of **a** GO **b** MG–NH_2–PEG. **c** Magnetic properties of MG–NH_2–PEG and MG–NH_2

experiments. The disinfection function of MG–NH_2–PEG: DOX at neutral and acidic (pH 4.4) pH conditions was incubated with MG–NH_2–PEG: DOX with 0.5 phosphate buffers. The unloaded DOX from MG–NH_2–PEG was centrifuged at different times followed by measurement of the supernatant fluorescence spectroscopy from MG–NH_2–PEG: DOX. Around 20% of DOX was released from nanocomposite with pH 7.4 whereas the release of DOX in acid buffer (pH 5.0) was almost 50% during 360 min. This was arisen from amino group protonation in the positively charged molecule of DOX, downgrading its impact with the hydrophobic surface of grapheme, and hence the drug delivery. In the MG–NH_2–PEG: DOX system, however, a significant test was found (about 10% at pH 7.4) in the first few minutes.

3.4. In vitro cytotoxicity

The MTT assay was carried out to ascertain the toxicity of both synthetic nanocomposites and the drug, (Mohammad-Taheri et al. 2012; Taylor 2015). Figure 7 shows the cell toxicity level and the absorption rate of synthesized nanocarrier by the synthetic MCF-7 cell. As a desirable result, the nanocomposite is acceptably non-toxic because cell survival percentage is over 85% after 48 h, with a cellular absorption rate of more than 80%, which is an.

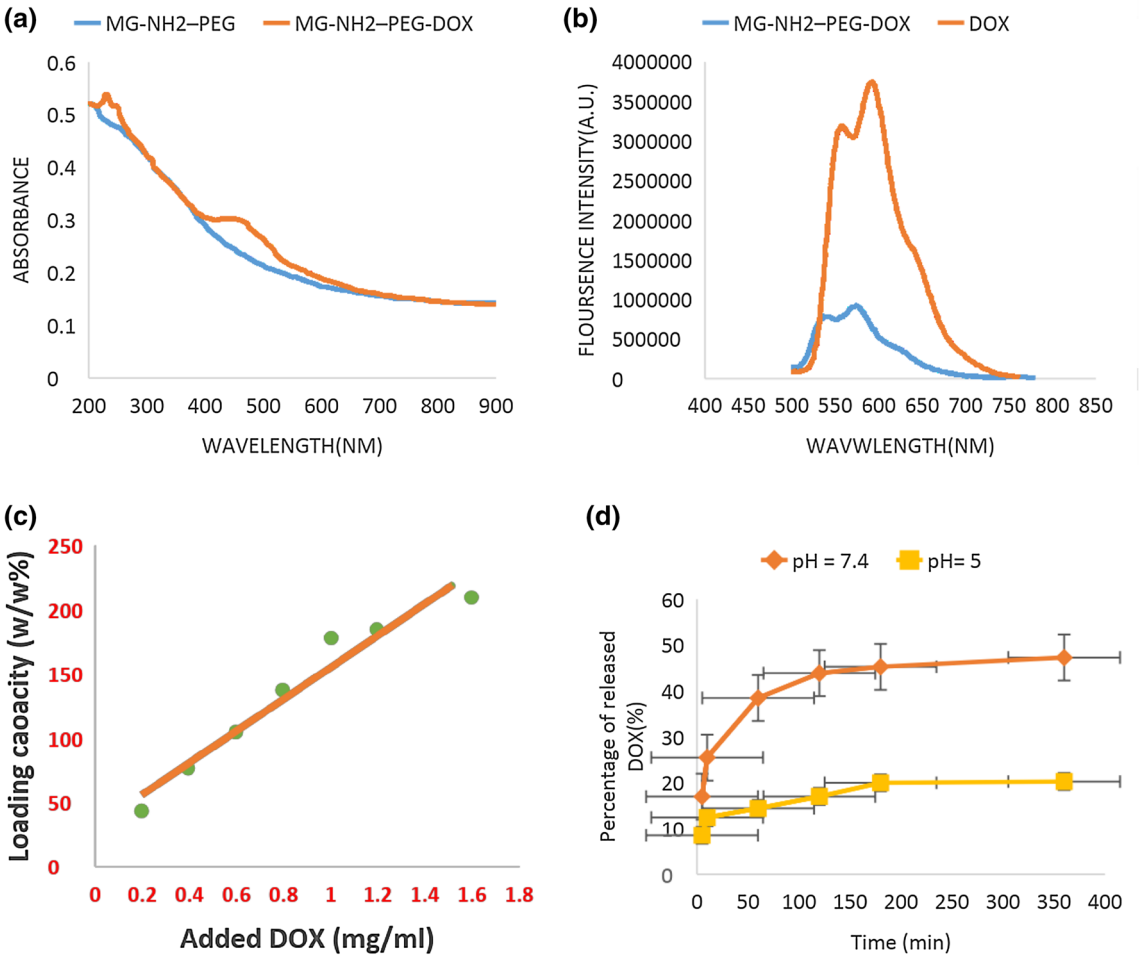

Fig. 6 Drug loading and release in the MG–NH_2–PEG: DOX system. **a** UV–VIS absorbance spectra of MG–NH_2–PEG and MG–NH_2–PEG: DOX. **b** Fluorescence spectra of free DOX and MG–NH_2–PEG: DOX at the same DOX concentration (5 µmol/l) under 490 nm excitation. **c** Quantification of DOX loading at different feeding amounts of DOX. The GO concentration was kept at 0.2 mg/ml in MG–NH_2–PEG samples. In the experiment, DOX loading maximized as much as ~ 220% by weight. **e** DOX release from MG–NH_2–PEG: DOX nanocomposite in buffers at pH 5.0 and 7.4 at a range of time points. Error bars indicate triplicate samples

3.5. Drug delivery using magnetically targeting methodology

A number of studies have reported recently the implementation of drug delivery using magnetic targeting approach (Kim et al. 2011; Jiang 2013; Gajendiran et al. 2019). Also numerous studies have demonstrated the effectiveness of retaining magnetic nanoparticles in tumor affected sites through an external magnetic field applied locally, and provide for magnetic targeting of tumors that way (Kiew 2017; Vila et al. 2012). MG–NH_2–PEG with its outstanding magnetic performance provides the possibility of using it as nanocarrier for drug delivery in magnetically targeting of tumor systems. We embedded a magnet underneath the in vitro cell culture and encouraged the local concentration of MG–NH_2–PEG: DOX, conducted through the applied magnetic field (Fig. 8a). Imaging through Confocal fluorescence for the DOX detection indicated high consumption of MG–NH_2–PEG–DOX by the cells that had grown up on the upper surface of the magnet system during the first 6 h of the observation; whereas very little DOX fluorescence was found in cells located at points distanced from the magnet system in that same culture dish. Imaging of cells via Calcein AM/PI double stained method following 24 h of incubation revealed the efficiency of selectively killing of cells located closer to the magnetic field under the effect of magnetically targeted drug delivery of MG–NH_2–PEG: DOX, meanwhile leaving the viability of cells outside the magnetic field intact (Fig. 8b).

3.6. Magnetically targeted photothermal therapy

One of the methods for inducing photothermal damage to the tumor cells exposed to NIR light is the application of

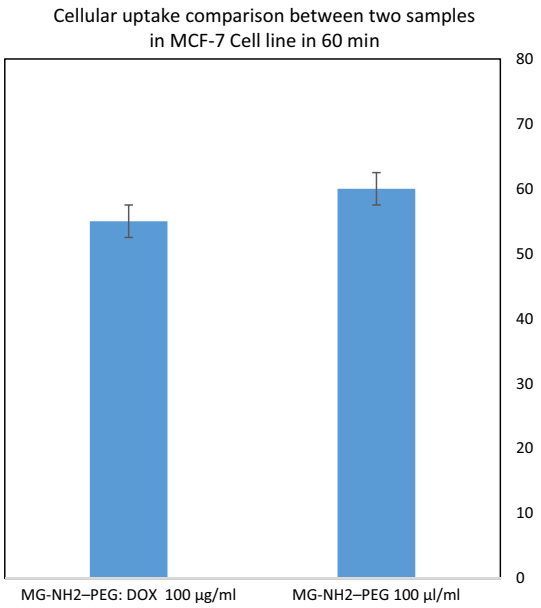

Fig. 7 In vitro cell toxicity tests: comparison of cellular uptake between two samples in MCF-7 Cell line within 48 h

light-absorbing agents; a method that is frequently used by PTT (Su et al. 2019). Research on PTT treatment of cancer during the past decade has explored numerous nanomaterial including nanostructures, carbon nanotubes, and nanographene in terms of their anticancer properties (Dissanayake et al. 2015; Ge 2014). MG–NH_2–PEG exclusively, features very strong optical absorption properties in NIR window; in fact, this unique property was what made the researcher to base this study on for investigating its photothermal effects on the ablation of cancer cells. A power density equal to 1 W/cm^2 was used to exposure MG–NH_2–PEG to an 808 nm NIR laser, resulting in rapid increase of its temperature pursuant to a concentration-dependent behavior, which was considerably contrary to the insignificant temperature change of water when observed under identical irradiation environment (Fig. 9a). Thus the main aim of this study was using the photothermal effect of MG–NH_2–PEG for photothermal ablation of cancer cells. After 2 h of incubation of MCF-7 cells with MG–NH_2–PEG, they were subjected to an 808 nm laser for 5 min meanwhile applying variable power densities. Then the MTT assessment was performed to identify the cells' relative viabilities afterwards the PTT treatment. Findings showed that although the untreated cells largely maintained their viabilities despite the higher laser irradiation (up to 2 W/cm^2), the best part of the cancer cells incubated by MG–NH_2–PEG were killed following the laser irradiation, representing decreased cell viabilities vs. the increase in the power of laser (Fig. 9b). The peculiar magnetic properties of MG–NH_2–PEG can then be exploited for the application of magnetically targeted PTT. In this study the MG–NH_2–PEG was used for the incubation of MCF-7 cells for a 2 h time span at 37 °C under the effect of a specified magnetic field. The cells treated by 20 min NIR laser irradiation, appeared differently, that is, the cells closer to the magnetic field had been significantly destroyed, whereas the ones located at further distance from the magnetic field remained largely unaffected (Fig. 9c).

Conclusions

The present study is the first to synthesize MG–NH_2–PEG nanocomposite demonstrating that:

1) A wide-range stability of graphene oxide is a result of the amino group function, which mediates the estab-

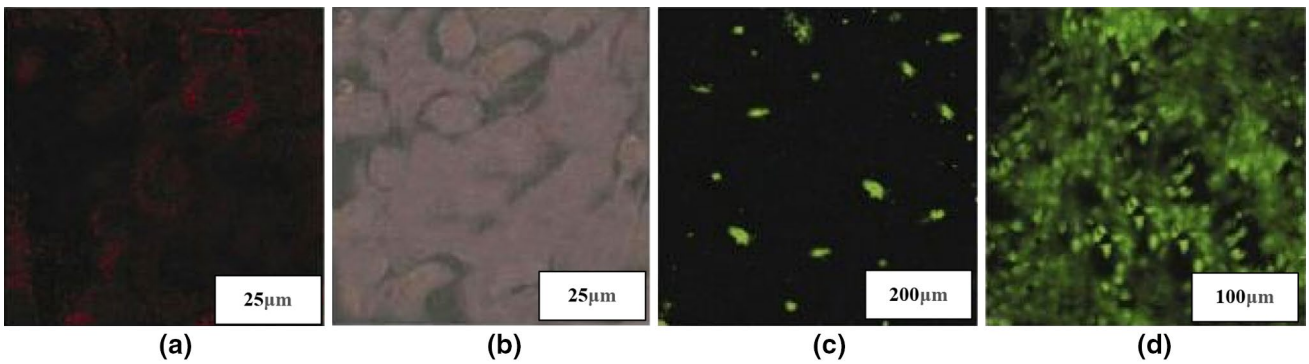

Fig. 8 Drug delivery to the magnetically targeted cells. **a** The cells located distanced from the magnetic field. **b** DOX fluorescence was observed in the above images, taken during following 6 h of incubation. Confocal images representing the Calcein AM/PI co-stained cells afterwards the incubation by MG–NH_2–PEG: DOX for 24 h, taken right above the magnetic field (**c**) and at distanced from the magnetic field (**d**). Calcein AM and PI was used respectively for the green and red staining of live and dead cells through the use of fluorescence microscope

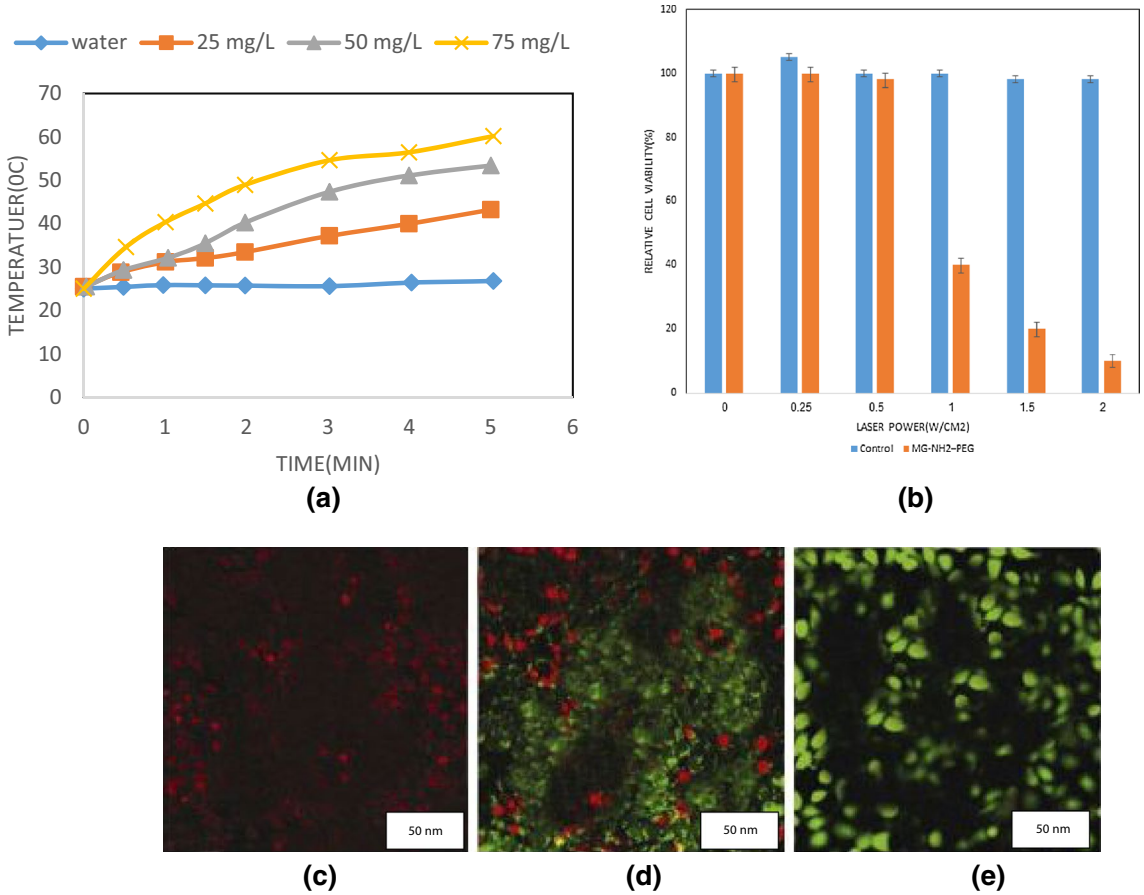

Fig. 9 Magnetically targeted cancer cells under photothermal ablation conditions. **a** Representations of water temperature changes and MG–NH_2–PEG (25, 50, 75 mg/l) concentration variability under 808 nm laser irradiation at 1 W/cm^2 power density for a 5 min time span; **b** MG–NH_2–PEG (50 mg/l) relative viabilities after treatment of MCF-7 cells and untreated control cells following irradiation with the NIR laser at various power densities for a 5 min. time span. **c** Above the magnet; **d** a location close to the magnetic field; **e** a location distanced from the magnetic field. Error bars represent four parallel samples

lishment of a bond with the carboxyl group polymeric polyethylene glycol carboxylate.

2) The amount of nanocomposite magnetism is reduced by polyethylene glycol polymer, however, it rises in biological conditions and lowers the substance toxicity.
3) The introduced nanoscale carrier is applicable as an appropriate choice for Doxorubicin as an anticancer drug, showing the best performance in pH 7.4.
4) MG–NH_2–PEG with its outstanding magnetic performance provides the possibility of using it as a nanocarrier for drug delivery in magnetically targeting of tumor systems.
5) A power density equal to 1 W/cm^2 was used to exposure MG–NH_2–PEG to an 808 nm NIR laser, resulting in rapid increase of its temperature pursuant to a concentration-dependent behavior, which was considerably contrary to the insignificant temperature change of water when observed under identical irradiation environment. Findings showed that although the untreated cells largely maintained their viabilities despite the higher laser irradiation (up to 2 W/cm^2), the best part of the cancer cells incubated by MG–NH_2–PEG were killed following the laser irradiation, representing decreased cell viabilities vs. the increase in the power of laser.

Acknowledgements The authors wish to acknowledge financial support provided for this work by the University of Tehran. Special thanks also go to the scientific help and guidance by Foad Soleimani, Mahan Rahmati, Ahmad Taiebi and Maryam Azarian.

Compliance with ethical standards

Conflict of interest There are no conflicts to declare.

References

Akbarzadeh A, Mikaeili H, Zarghami N, Mohammad R, Barkhordari A, Davaran S (2012) Preparation and in vitro evaluation of doxorubicin-loaded Fe3O4 magnetic nanoparticles modified with biocompatible copolymers. Int J Nanomed 7:511–526

Akhavan O, Ghaderi E (2010) Toxicity of graphene and graphene oxide nanowalls against bacteria. ACS Nano 4(10):5731–5736

Angelopoulou A, Voulgari E, Diamanti EK, Gournis D, Avgoustakis K (2015) Graphene oxide stabilized by PLA-PEG copolymers for the controlled delivery of paclitaxel. Eur J Pharm Biopharm 93:18–26

Baniasadi H, Ramazani SA, Mashayekhan S, Ramezani Farani M, Ghaderinezhad F, Dabaghi M (2015) Design, fabrication, and characterization of novel porous conductive scaffolds for nerve tissue engineering. Int J Polym Mater Polym Biomater 64(18):969–977

Cole AJ, David AE, Wang J, Galbán CJ, Yang VC (2011) Magnetic brain tumor targeting and biodistribution of long-circulating PEG-modified, cross-linked starch-coated iron oxide nanoparticles. Biomaterials 32(26):6291–6301

Costantini S, Di Bernardo G, Cammarota M, Castello G, Colonna G (2013) Gene expression signature of human HepG2 cell line. Gene 518(2):335–345

Dinesh B, Devi KS, Kumar AS (2017) Curcumin-quinone immobilised carbon black modified electrode prepared by in-situ electrochemical oxidation of curcumin-phytonutrient for mediated oxidation and flow injection analysis of sulfide. J Electroanal Chem 804:116–127

Depan D, Shah J, Misra RDK (2011) Controlled release of drug from folate-decorated and graphene mediated drug delivery system: synthesis, loading efficiency, and drug release response. Mater Sci Eng C 31(7):1305–1312

Dissanayake NM, Current KM, Obare SO (2015) Mutagenic effects of iron oxide nanoparticles on biological cells. Int J Mol Sci 16(10):23482–23516

El-boubbou K (2018) Magnetic iron oxide nanoparticles as drug carriers: clinical relevance. Nanomedicine (Lond) 13(8):953–971. https://doi.org/10.2217/nnm-2017-0336

Farani R et al (2019) Extending the application of a magnetic PEG three-part drug release device on a graphene substrate for the removal of Gram-positive and Gram-negative bacteria and cancerous and pathologic cells. Drug Des Devel Ther 13:1581–1591

Feng L, Liu Z (2011) Graphene in biomedicine: opportunities and challenges. Nanomedicine 6(2):317–324

Gajendiran M, Jo H, Kim K (2019) Green synthesis of multifunctional PEG-carboxylate π back-bonded gold nanoconjugates for breast cancer treatment. Int J Nanomed. https://doi.org/10.2147/IJN.S190946

Garg B, Bisht T, Ling YC (2015) Graphene-based nanomaterials as efficient peroxidase mimetic catalysts for biosensing applications: an overview. Molecules 20(8):14155–14190

Ge J et al (2014) A graphene quantum dot photodynamic therapy agent with high singlet oxygen generation. Nat Commun 5:4596

Guo L et al (2016) Prostate cancer targeted multifunctionalized graphene oxide for magnetic resonance imaging and drug delivery. Carbon N Y 107:87–99

Hong BJ, Compton OC, An Z, Eryazici I, Nguyen ST (2011) Successful stabilization of graphene oxide in electrolyte solutions: enhancement of bio-functionalization and cellular uptake. ACS Nano 127:1–10

Huang J et al (2012) Mechanism of cellular uptake of graphene oxide studied by surface-enhanced Raman spectroscopy. Small 8(16):2577–2584

Hu CS, Tang SL, Chiang CH, Hosseinkhani H, Da Hong P, Yeh MK (2014) Characterization and anti-tumor effects of chondroitin sulfate–chitosan nanoparticles delivery system. J Nanoparticle Res 16(11):2672

Jiang F et al (2013) Eco-friendly synthesis of size-controllable amine-functionalized graphene quantum dots with antimycoplasma properties. Nanoscale 5(3):1137

Kim Y, Kim M, Min D (2011) Biocompatible reduced graphene oxide prepared by using dextran as a multifunctional reducing agent w. 3195–3197

Kumawat MK, Thakur M, Gurung RB, Srivastava R (2017) Graphene quantum dots from mangifera indica: application in near-infrared bioimaging and intracellular nano-thermometry. ACS Sustain Chem Eng 5(2):1382–1391. https://doi.org/10.1021/acssuschemeng.6b01893

Kiew SF et al (2017) Preparation and characterization of an amylase-triggered dextrin-linked graphene oxide anticancer drug nanocarrier and its vascular permeability. Int J Pharm 534(1–2):297–307

Li S, Xiao L, Deng H, Shi X, Cao Q (2017) Remote controlled drug release from multi-functional Fe_3O_4/GO/Chitosan microspheres fabricated by an electrospray method. Colloids Surf B Biointerfaces 151:354–362

Lu Y-J, Wei K-C, Ma C-CM, Yang S-Y, Chen J-P (2012) Dual targeted delivery of doxorubicin to cancer cells using folate-conjugated magnetic multi-walled carbon nanotubes. Colloids Surf B Biointerfaces 89:1–9

Liu J, Dong J, Zhang T, Peng Q (2018) Graphene-based nanomaterials and their potentials in advanced drug delivery and cancer therapy. J. Control. Release 286(May):64–73

Liao KH, Lin YS, MacOsko CW, Haynes CL (2011) Cytotoxicity of graphene oxide and graphene in human erythrocytes and skin fibroblasts. ACS Appl Mater. Interfaces 3(7):2607–2615

Ma X et al (2012) A functionalized graphene oxide-iron oxide nanocomposite for magnetically targeted drug delivery, photothermal therapy, and magnetic resonance imaging. Nano Res 5(3):199–212

Mehnati-najafabadi V, Taheri-kafrani A, Bordbar A (2018) Xylanase immobilization on modified superparamagnetic graphene oxide nanocomposite: effect of PEGylation on activity and stability. Int J Biol Macromol 107:418–425

Markovic ZM et al (2011) In vitro comparison of the photothermal anticancer activity of graphene nanoparticles and carbon nanotubes. Biomaterials 32(4):1121–1129

Marković ZM et al (2017) Ambient light induced antibacterial action of curcumin/graphene nanomesh hybrids. RSC Adv 7(57):36081–36092

Mendonça MCP et al (2016) PEGylation of reduced graphene oxide induces toxicity in cells of the blood-brain barrier: an in vitro and in vivo study. Mol Pharm 13(11):3913–3924

Mohammad-Taheri M, Vasheghani-Farahani E, Hosseinkhani H, Shojaosadati SA, Soleimani M (2012) Fabrication and characterization of a new MRI contrast agent based on a magnetic dextran–spermine nanoparticle system. Iran Polym J 21(4):239–251

Ozcan F, Ersoz M, Yilmaz M (2009) Preparation and application of calix[4]arene-grafted magnetite nanoparticles for removal of dichromate anions. Mater Sci Eng C 29(8):2378–2383

Ordikhani F, Farani MR, Dehghani M, Tamjid E, Simchi A (2015) Physicochemical and biological properties of electrodeposited

graphene oxide/chitosan films with drug-eluting capacity. Carbon 84:91–102
Qiao R et al (2018) Bioconjugation and Fluorescence Labelling of Iron Oxide Nanoparticles Grafted with Bromomaleimide- terminal Polymers. Biomacromol 19:4423–4429
Skwarecki AS, Milewski S, Schielmann M, Milewska MJ (2016) Antimicrobial molecular nanocarrier–drug conjugates. Nanomed Nanotechnol Biol Med 12(8):2215–2240
Sablok K, Bhalla V, Sharma P, Kaushal R, Chaudhary S, Suri CR (2013) Amine functionalized graphene oxide/CNT nanocomposite for ultrasensitive electrochemical detection of trinitrotoluene. J Hazard Mater 248–249(1):322–328
Singh SK, Singh MK, Kulkarni P, Sonkar VK, Gracio J (2012) Amine-modified graphene: thrombo-protective safer alternative to graphene oxide for biomedical. ACS Nano 6(3):2731–2740
Su X, Tao J, Wang Q, Xu P, Luo W, Dang M, Wu J, Teng Z (2019) Controlled PEGylation of periodic mesoporous organosilica nanospheres for improving their stability in physiological solutions. Chin Chem Lett 30(4):929–932. https://doi.org/10.1016/j.cclet.2019.02.014
Sun X, Zebibula A, Dong X, Zhang G, Zhang D, Qian J, He S (2018) Aggregation-induced emission nanoparticles encapsulated with PEGylated nano graphene oxide and their applications in two-photon fluorescence bioimaging and photodynamic therapy in vitro and in vivo. ACS Appl Mater Interfaces 10(30):25037–25046. https://doi.org/10.1021/acsami.8b05546
Tao C, Zheng Q, An L, He M, Lin J, Tian Q, Yang S (2019) T 1-weight magnetic resonance imaging performances of iron oxide nanoparticles modified with a natural protein macromolecule and an artificial macromolecule. Nanomaterials (Basel) 92(2):170. https://doi.org/10.3390/nano9020170
Taylor P (2015) International journal of polymeric materials and design, fabrication, and characterization of novel porous conductive scaffolds for nerve tissue engineering design, fabrication, and characterization of novel porous conductive scaffolds for nerve tissue engineering 37–41.
Vila M, Portolés MT, Marques PA, Feito MJ, Matesanz MC, Ramírez-Santillán C, Gonçalves G, Cruz SM, Nieto A, Vallet-Regi M (2012) Cell uptake survey of pegylated nanographene oxide. Nanotechnology 23(46)
Wilding KM, Smith AK, Wilkerson JW, Bush DB, Knotts TA 4th, Bundy BC (2018) The locational impact of site-specific PEGylation: streamlined screening with cell-free protein expression and coarse-grain simulation. The locational impact of site-specific PEGylation: streamlined screening with cell-free protein expression and coarse-grain simulation. ACS Synth Biol 7(2):510–521. https://doi.org/10.1021/acssynbio.7b00316
Xie B et al (2017) Characterization of synergistic anti-tumor effects of doxorubicin and p53 via graphene oxide-polyethyleneimine nanocarriers. J Mater Sci. Technol 33(8):807–814
Yuan G, Yuan Y, Xu K, Luo Q (2014) Biocompatible PEGylated Fe3O4 nanoparticles as photothermal agents for near-infrared light modulated cancer therapy. Int J Mol Sci 15(10):18776–18788
Zhao X, Shang T, Zhang X, Ye T, Wang D, Rei L (2016) Passage of magnetic tat-conjugated Fe_3O_4@SiO_2 nanoparticles across in vitro blood–brain barrier. Nanoscale Res Lett 11(1):451. https://doi.org/10.1186/s11671-016-1676-2